Available online at BCREC website: https://bcrec.id

Bulletin of Chemical Reaction Engineering & Catalysis, 17 (3) 2022, 508-519

Research Article

Photooxidation and Virus Inactivation using TiO_2(P25)–SiO_2 Coated PET Film

Chaowat Autthanit[1], Supachai Jadsadajerm[2], Oswaldo Núñez[3], Purim Kusonsakul[3], Jittima Amie Luckanagul[4], Visarut Buranasudja[5], Bunjerd Jongsomjit[3], Supareak Praserthdam[6], Piyasan Praserthdam[3,*]

[1]*Department of Sustainable Industrial Management Engineering, Faculty of Engineering, Rajamangala University of Technology Phra Nakhon. Bangkok 10800. Thailand.*
[2]*Department of Industrial Chemistry, Faculty of Applied Science, King Mongkut's University of Technology of North Bangkok, Bangkok 10800, Thailand.*
[3]*Center of Excellence on Catalysis and Catalytic Reaction Engineering. Department of Chemical Engineering, Faculty of Engineering, Chulalongkorn University. Bangkok 10330. Thailand.*
[4]*Department of Pharmaceutics and Industrial Pharmacy and Research Unit for Plant-produced Pharmaceuticals, Faculty of Pharmaceutical Sciences, Chulalongkorn University. Bangkok 10330. Thailand.*
[5]*Department of Pharmacology and Physiology, Faculty of Pharmaceutical Sciences, Chulalongkorn University. Bangkok 10330. Thailand.*
[6]*Performance Computing Unit (CECC-HCU), Center of Excellence on Catalysis and Catalytic Reaction Engineering (CECC), Chulalongkorn University. Bangkok 10330. Thailand.*

Received: 6th May 2022; Revised: 22nd June 2022; Accepted: 23rd June 2022
Available online: 4th July 2022; Published regularly: September 2022

Abstract

This study chemically modified PET film surface with P25 using silicate as a binder. Different P25–binder ratios were optimized for the catalyst performance. The modified samples were analyzed by scanning electron microscopy-energy-dispersive X-ray spectroscopy and Fourier transform infrared spectroscopy. Diffuse reflectance UV-vis spectra revealed significant reductions in the band gaps of the P25 solid precursor (3.20 eV) and the surface-modified PET–1.0Si–P25 (2.77 eV) with visible light. Accordingly, under visible light conditions, catalyst activity on the film will occur. Additionally, the film's performance was evaluated using methylene blue (MB) degradation. Pseudo-first-order-rate constants (min^{-1}), conversion percentages, and rates ($\mu g.mL^{-1}.g_{cat}^{-1}.h^{-1}$) were determined. The coated films were evaluated for viral ***Phi–X 174*** inactivation and tested with fluorescence and UV-C light illumination, then log (N/N_0) versus t plots (N = [virus] in plaque-forming units [PFUs]/mL) were obtained. The presence of nanosilica in PET showed a high adsorption ability in both MB and ***Phi–X 174***, whereas the best performances with fluorescent light were obtained from PET–1.0Si–P25 and PET–P25–1.0Si–SiO_2 equally. A 0.2-log virus reduction was obtained after 3 h at a rate of 4×10^6 $PFU.mL^{-1}.g_{cat}^{-1}.min^{-1}$. Additionally, the use of this film for preventing transmission by direct contact with surfaces and via indoor air was considered. Using UV light, the PET–1.0Si–P25 and PET–1.0Si–P25–SiO_2 samples produced a 2.5-log inactivation after 6.5 min at a rate of 9.6×10^6 and 8.9×10^6 $PFU.mL^{-1}.g_{cat}^{-1}.min^{-1}$, respectively.

Keywords: Photooxidation; virus inactivation; PET film; P25 titania; P25-silica

How to Cite: C. Autthanit, S. Jadsadajerm, O. Núñez, P. Kusonsakul, J.A. Luckanagul, V. Buranasudja, B. Jongsomjit, S. Praserthdam, P. Praserthdam (2022). Study Photooxidation and Virus Inactivation using TiO_2(P25)–SiO_2 Coated PET Film. *Bulletin of Chemical Reaction Engineering & Catalysis*, 17(3), 508-519 (doi: 10.9767/bcrec.17.3.14180.508-519)

Permalink/DOI: https://doi.org/10.9767/bcrec.17.3.14180.508-519

1. Introduction

Microorganisms, such as viruses, fungi, and bacteria, can be removed efficiently and economically using photocatalytic oxidation–reduction (redox). This process uses a semiconductor as a catalyst and artificial or solar light as an energy source to induce simultaneously occurring oxidation and reduction processes at the catalyst's surface. In this heterogeneous catalytic process [1–3], an electron is excited by the light energy

* Corresponding Author.
Email: piyasan.p@chula.ac.th (P. Praserthdam);
Telp: +66-2218-6861 Fax. 66-2218-6877

from a semiconductor valence band (VB) to the corresponding conduction band (CB); consequently, a carrier pair (*e*/*h*) is formed at the CB and VB, respectively. After the carriers separate, they migrate to the catalyst's surface, and simultaneous electron transfer occurs from and to the electrolytes. At the CB, electrons are transferred to O_2 to produce superoxide radical anions that become further reduced to HOOH and water. Simultaneously, at the VB, hydroxyl radical (OH.) electrons are transferred from water to the catalyst. In both cases, reactive oxygen species (ROS) are formed; these react with the membranes of microorganisms, thereby inducing the oxidation of the membrane and causing the destruction of the microorganism (Figure 1). The microorganism removal efficiency [4] (Q) can be obtained by measuring $-\log(N/N_0)$, where N and N_0 are the microorganism concentrations at time t and time 0 (initial); for viruses, this is measured in terms of plaque-forming units (PFUs) per milliliter. Typically, the efficiency of a decontamination process in reducing the concentration of a contaminant is measured using a log reduction scale; therefore, efficiency is measured as the number of log units, e.g. n = 1, 2, and 3 represent 90%, 99%, and 99.9% removal efficiency, respectively.

Nonhazardous and highly stable *n*-type semiconductors have been used to disinfect microorganisms, including TiO_2, CuO, and ZnO. Previously, an increase in photocatalytic activity was noted with the addition of SiO_2 to TiO_2; the activity resulted from enhanced microorganism adsorption on the surface of TiO_2, reduced e/h recombination, and increased OH [5]. Additionally, a review of the photocatalytic inactivation for waterborne, airborne, and food-borne viruses has recently been published [6]. Most of the reported cases used UV-C and UV-A (black light blue) on different viruses with variable log reductions, with most using powders as catalysts. However, few cases of catalyst-coated films have been reported, e.g. films coated in TiO_2/CuO [7] and g-WO_3 [8]. In [7], T4 phages were treated using a 40 W UV-A lamp (log of 9.9 in 80 min), whereas in literature [8], MS2 phages were treated with a mercury lamp (5.9 log in 180 min). Generally, there have been few reports on studies using solar or visible light.

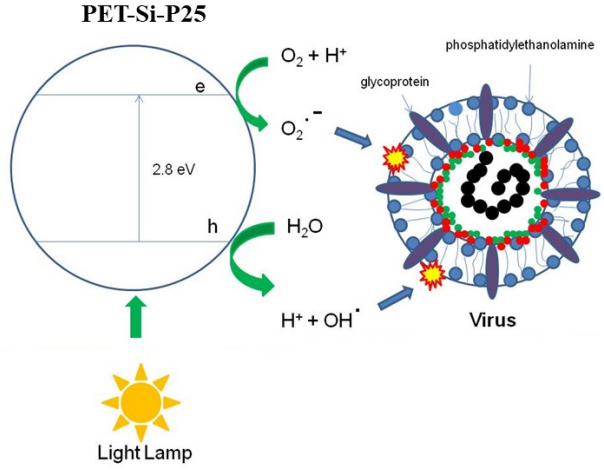

Figure 1. Virus inactivation via ROS ($OH^{\cdot}$ and $O_2^{\cdot -}$) membrane oxidation.

TiO_2 has attracted more and more interest due to its great advantages, including water splitting, pollutant degradation, solar cell, lithium-ion batteries as well as photocatalyst. Electronic structure and consequently magnetic and optical properties of TiO_2 nanoparticles can be changed by doping with nickel, chromium, iron, vanadium, zinc, etc. [9]. Doping allows for changes in the electronic structure of TiO_2 nanoparticles, as well as changes in their chemical composition and optical properties [10]. The synthesis method to produce TiO_2 thin films and the substrate on which it is deposited is known to play an important role for design efficacy of a biomaterial. A scratch-resistant coating method using wash coating and screen printing techniques to coat stainless steel and aluminum plates with TiO_2 has been reported, and antimicrobial activity has been tested using UV light [11]. Additionally, TiO_2 nanoparticles have been attached to polymers using techniques including liquid phase deposition, dip coating, spreading, and chemical attachment, whereas reduction, emulsion polymerization, atom transfer, and radical polymerization have also been described [12–17]. Indeed, TiO_2 nanoparticles have been grafted to polymethyl methacrylate film using the latter technique [18].

Organic polymers have potentially wide applicability as flexible substrates for the deposition of photocatalytic films, given the ease in which they can be formed into shapes post-deposition. Polyethylene terephthalate (PET) is recyclable and it is considered one of the most important engineering plastics owing to its excellent tensile and impact strength, chemical resistance, clarity, processability, colourability and reasonable thermal stability. Moreover, the TiO_2 thin films deposited onto PET substrates might work as a UV-protective layer, since they absorb UV light, increasing the life time of the polymeric material [19]. In addition, viruses and its host bacteria are usually co-existent in real water environment, but few

related researches have been conducted to study the interaction between them in photocatalytic systems, so it is of practical significance to investigate the photocatalytic inactivation efficiency in ***Phi–X 174*** virus system using surface-modified SiO_2 chemically coated with TiO_2 on PET film.

In this context, this study reports different conditions for surface-modified SiO_2 chemically coated with TiO_2 on PET film. The coated film samples were tested for UV light photooxidation using methylene blue (MB) degradation at a neutral pH. The best-performing film was characterized by scanning electron microscopy with Energy-dispersive X-ray spectroscopy (SEM-EDX), Fourier transform infrared (FT-IR) spectroscopy, photoluminescence (PL) spectroscopy, the Brunauer–Emmett–Teller (BET) method, and UV-vis reflectance spectroscopy. This film was tested for the inactivation of the ***Phi–X 174*** bacteriophage under 2,000-lux fluorescent and 18 W UV-C lights. This study discusses the kinetics of oxidation and virus inactivation and their consequences and offers recommendations on virus deactivation applications.

2. Materials and Methods

2.1 Materials

This study used the following chemicals and materials: TiO_2 (P25) Aeroxide and tetraethyl orthosilicate (TEOS) (98%) were obtained from Aldrich, deionized (DI) water and ethyl alcohol (99.9%) were supplied by QReC, and fuming hydrochloric acid (37%) was obtained from Merck. Silicon dioxide (SiO_2) nanopowders (5–15 nm) (99.5%) were supplied by Sigma–Aldrich. The Nabsolute company limited supplied both the ***Phi–X174*** virus and the ***E. Coli*** bacteria. Agar, 125 μm high-quality large-format PET film roll, and cultivation plates (90×150 mm) were obtained from Hycon Plastics. Methylene blue (MB, $C_{16}H_{18}ClN_3S$) was purchased from Unilab. Micropipettes (2–20, 20–200, and 100–1,000 μL) were supplied by Gilson. Nutrient broth agar was obtained from Conda, and KCl was supplied by Kemaus. American bacteriological agar and $CaCl_2$ were obtained from Conda and Bio Basic, respectively.

2.2 Equipment

The morphology and crystalline structure were examined via SEM-EDX using an AMICUS photoelectron spectrometer with an Mg-K_α X-ray source controlled by KRATOS Vision2 software with a current of 20 mA and an energy of 10 keV. The binding energy was calibrated by the C 1s peak at 284.6 eV. Ti 2p and O 1s peaks were observed at 455–470 and 525–540 eV, respectively. Diffuse reflectance (DRS) UV-vis spectra were recorded on a Perkin Elmer Lambda-650 instrument. The sample (ca. 200–300 mg) was loaded into a quartz cell under normal condition, and the spectra were collected in the wavelength range from 200-800 nm with a step size at 1 nm reference to $BaSO_4$. Light absorption data were obtained using UV Win Lab software (PerkinElmer). The band gaps were calculated using Tauc's equation, $(ahv)^{1/n} = A(hv-E_g)$, in which A is the optical constant, h is Planck's constant, a is the absorption coefficient, v is c/λ (in which c is the speed of light in a vacuum and λ is the wavelength), Eg is the optical band gap, and n is 0.5 and 2 for direct and indirect transitions, respectively. X-ray photoelectron spectroscopy analysis was employed to obtain insights about the chemical state in the catalyst surface. For all elements, there is a characteristic of binding energy associated with each core atomic orbital. XPS was acquired using the AMICUS spectrometer with Al-K_α spectrometer (Thermo VG, USA) equipped with an Al-K_α X-ray radiation (1486.6 eV) at voltage 15kV and current of 12 mA. The pressure in the analysis chamber was less than 10^{-5} Pa. Charge referencing was measured against adventitious carbon (C 1s at 284.8 eV). Methylene blue (MB) was used for photo oxidation in a batch reactor comprising two Pyrex cylinders with different diameters; the cylinder with the smaller diameter contained a UV lamp and was immersed in the solution. The concentration of MB for different reactions was measured using a Varian Cary 5000 UV-Vis-near-infrared spectrophotometer, and the pH of the reactions was monitored using a Metter Toledo SevenMulti™ pH meter. The study used a sonicator from T. Ultrasonic Engineering Co., LTD., and an orbital oven temperature-controlled chamber (for incubation) from Biosan. An HVA-110 autoclave (Hirayama Manufacturing Corporation) and a Biosan ES-20 shaker–incubator were also used. Preliminary testing to detect microorganisms on the surface of the films was conducted using a Lumitester Smart A3 detector (ATP + ADP + AMP).

2.3 Film Preparation

2.3.1 PET–Si–P25 film

To prepare the films, 0.5, 1, or 1.5 mL TEOS was added (while stirring) to a solution con-

taining 35 mL of ethanol and 35 mL DI water until a final pH of 3 was reached. The solution was stirred magnetically for 15 min. To the final solution, 1 g P25 was added, and the solution was stirred for 24 h. The PET film was submerged in the final mixture and sonicated for 45 min. Both sides of the coated film were cleaned with a soft sponge and air dried for 15 min at 110 °C.

2.3.2 PET–1.0Si–P25–SiO_2 Film

A 1 mL volume of TEOS was added by stirring into a solution of 35 mL of DI water and 35 mL ethanol until a final pH of 3 was reached. Magnetic stirring continued for 15 min. P25 (1 g) and nanosilica (0.05 g) were added to the final solution and stirred for 24 h. The PET film was submerged in the final mixture and sonicated for 45 min. Both sides of the coated film were cleaned with a soft sponge and air dried for 15 min at 110 °C.

2.4 Virus and Bacteria Preparation

2.4.1 Culture media for the virus and bacteria

The nutrient broth on agar was added onto a plate, and 20 mL bottom agar was added and evenly distributed. Then, the agar solidification culture media was incubated at 37 °C.

2.4.2 Preparation of ***E. Coli***

The nutrient broth culture media (5 mL) was added into a 15 mL tube containing ***E. Coli*** (Nabsolute company limited). A colony of ***E. Coli*** was produced after overnight incubation in a shaker at 37 °C.

2.4.3 Preparation of the ***Phi–X 174*** virus

The ***Phi–X 174*** virus (Nabsolute company limited) was incubated using a procedure similar to the above method for ***E. Coli***.

2.5 Methylene Blue Oxidation Test

An area of PET–Si–P25 film (50 cm^2) was prepared by adding 0.5, 1, or 1.5 mL TEOS and 1 g P25 to a reactor containing 100 mL of a 4 ppm methylene blue (MB) water solution. The solution was stirred for 30 min before a UV light was activated. Then, a first aliquot sample (2.5 mL) was obtained. After the UV light had been activated, 2.5 mL aliquot samples were obtained every 15 min for 2 h. The remaining MB contained in each aliquot at each time interval was determined via UV-vis spectroscopy by measuring the corresponding absorbance signal at 668 nm. The corresponding rates and rate constants were obtained using absorbance measurements (or MB) (from the calibration curve).

2.6 Testing the Antiviral Properties of the Film

2.6.1 Testing procedure

The coated film and the blank (control) film samples were installed individually on the block tester. To prevent viral leakage, the block's screws were tightened firmly. Then, the block tester was disinfected under a hood of UV-C light for 15 min. A 2 µL volume of ***Phi–X 174*** was added dropwise into 5 mL of nutrient broth and mixed with Vortex. The mixture was transferred onto each block film where it was exposed to light (fluorescent or UV-C) for 30, 60, 120, and 180 min. Then, the reaction mixtures were added to two tubes (sample and control films). The mixtures were serially diluted with 90 µL nutrient broth and 10 µL of the mixture to achieve the required number of phages for the measurement (*i.e.*, until the phages could be counted). A 100 µL volume of the prepared bacteria was added to 10 µL of the mixture. Agar was poured on top until its total volume was 3 mL. Then, the mixture was transferred evenly onto a plate. Three controls and sample plates were prepared (for each testing time). After the agar had solidified, the samples were incubated overnight at 37 °C.

2.6.2 Analysis procedure

The total number of phages on the plates was counted, and the average (AVG) number was calculated. If necessary, different dilutions were used. The concentration of the virus was obtained according to the following calculation: concentration ($PFU.mL^{-1}$) = AVG number of phages × dilution factor × 100.

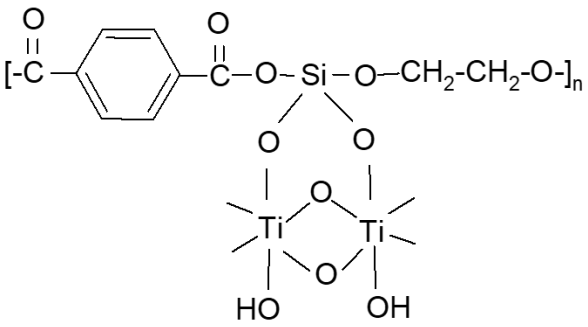

Figure 2. PET-Si-P25 proposed structure showing the Si binder chemical bonds to PET and P25.

3. Results and Discussion

3.1 Film Preparation and Characterization

PET film comprises esters of terephthalate and ethylene groups ([–$COC_6H_5CO–OCH_2CH_2–O–$]$_n$), and partial hydrolysis in an acidic media at the polymer's surface will yield [–COC_6H_5COOH $HOCH_2CH_2–O–$]$_n$. Thus, alcohol and acid groups are available to form chemical bonds at the surface of the polymer. Under this acidic condition, the addition of TEOS will cause the chemical attachment of silicate to the film ([–$COC_6H_5CO–OSi(OH)_2–OCH_2–CH_2–O–$]$_n$), leaving two OHs that can be attached to TiO_2. This study used this procedure to chemically coat PET film with P25 (Figure 2).

The addition of silicate–P25 to the resultant PET film's surface was verified via SEM-EDX and FT-IR spectroscopy. Table 1 presents the weight percentages of Ti and Si according to the quantities of TEOS used in the preparation. Figures 3, 4, and 5 show the SEM images, Tauc's equation using the DRS UV-vis spectra of the P25 powder and PET–1.0Si–P25, and the FT-IR spectra of PET, the P25–SiO_2 powder, and PET–1.0Si–P25 with the corresponding assignment of signals, respectively [20,21]. The plot of $(ahv)^2$ versus the photoenergy (hv) of each catalyst shown the curve line using the Tauc's relation (Figure 4), which intercepted on the photoenergy as its bandgap energy. The P25 powder had the wider energy bandgap about 3.20 eV, compared to the coated P25 on PET film that had the energy bandgap about 2.77 eV. The narrower energy bandgap of coat-

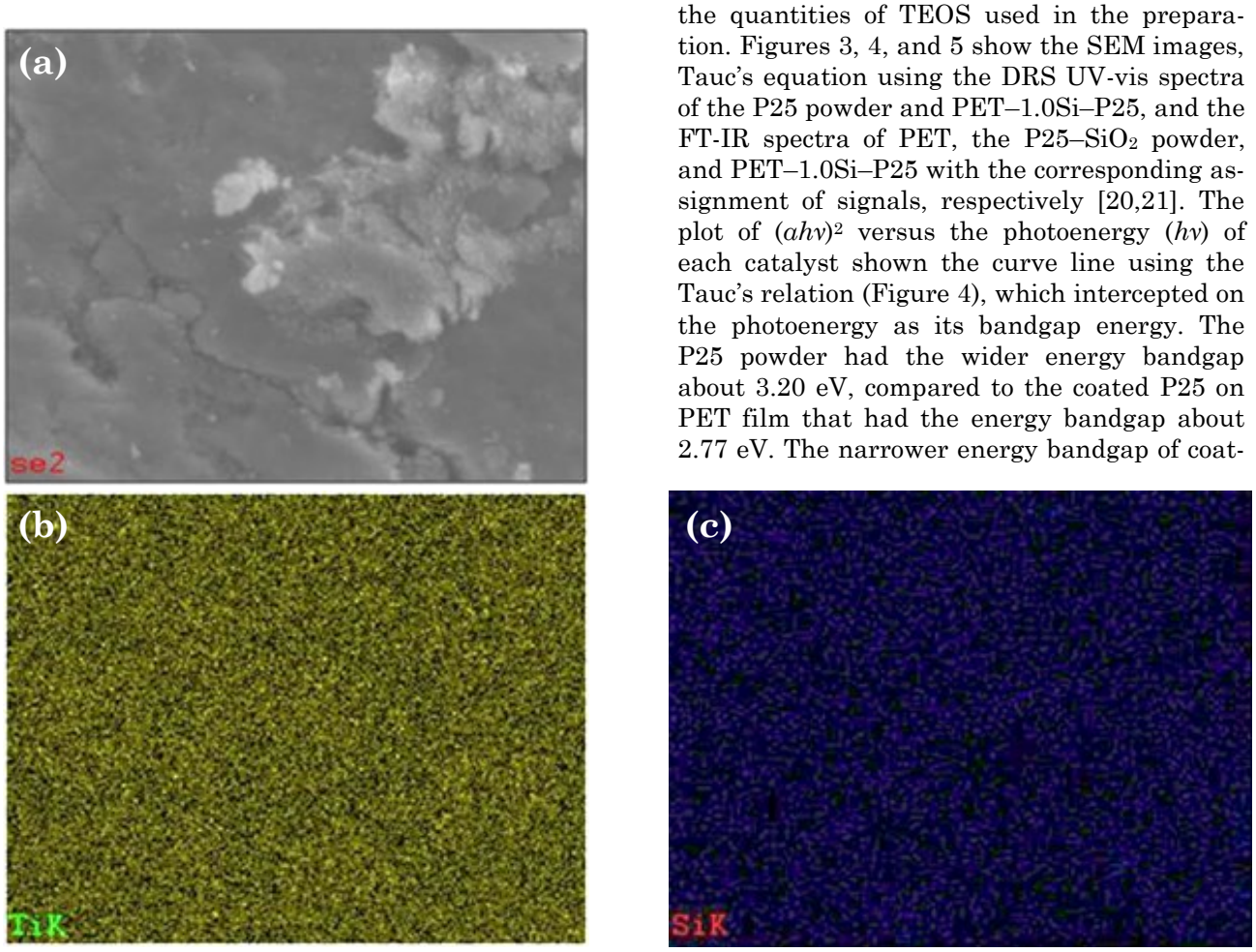

Figure 3. SEM images of PET–1.0Si–P25 showing (a) surface, (b) Ti distribution and (c) Si distribution.

Table 1. MB degradation using P25 on PET films prepared under different conditions. P25 attached on film without SiO_2 binder was also tested. Pseudo-first order rate constants and rates are also shown.

Catalyst films total catalyst weight of 50 cm^2 of film: 0.01 g	%wt on film		Band gap E_g (eV)	% Conversion		k_{obs} (min^{-1}) (half-time; min)	rate ($mg.mL^{-1}.g_{cat}^{-1}.h^{-1}$)
	Ti	Si		30 min	45 min		
PET-P25	12.8	0.0	3.2	7.1	9.7	[c]	[c]
PET-0.5Si-P25	52.7	1.7	2.77	25.1	35.2	0.015 (20)	[c]
PET-1.0Si-P25	55.3	3.8		30.2	43.9	0.02 (15)[a]	85[b]
PET-1.5Si-P25	45.7	6.4		17.6	29.6	0.01 (30)	[c]
PET-1.0Si-P25-SiO_2	53.0	4.4		39.0	52.2	[c]	[c]

[a] Same value obtained by plotting $\ln(-(Abs_{inf}-Abs_t))$ vs. time and $\ln([MB]_t/[MB]_0)$ vs. time.
[b] Obtained from the [MB] consumed after 2 h (1.69 ppm = 1.69 $mg.mL^{-1}$) divided by 2 h and 0.01 g_{cat}
[c] Not measured.

ed film resulted in the electrons transferred from the valence band to the conduction band more efficiently. Table 1 also presents the band gaps, e.g. corresponding to PET–1.0Si–P25. The band gaps of PET–1.0Si–P25 are significantly lower than those of P25; thus, it is expected that catalyst activity in the visible region will occur.

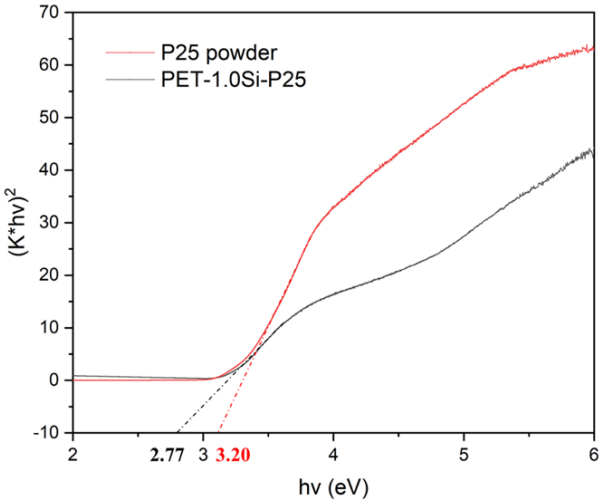

Figure 4. Band gap values of P25 powder and PET–1.0Si–P25 using Tauc´s equation.

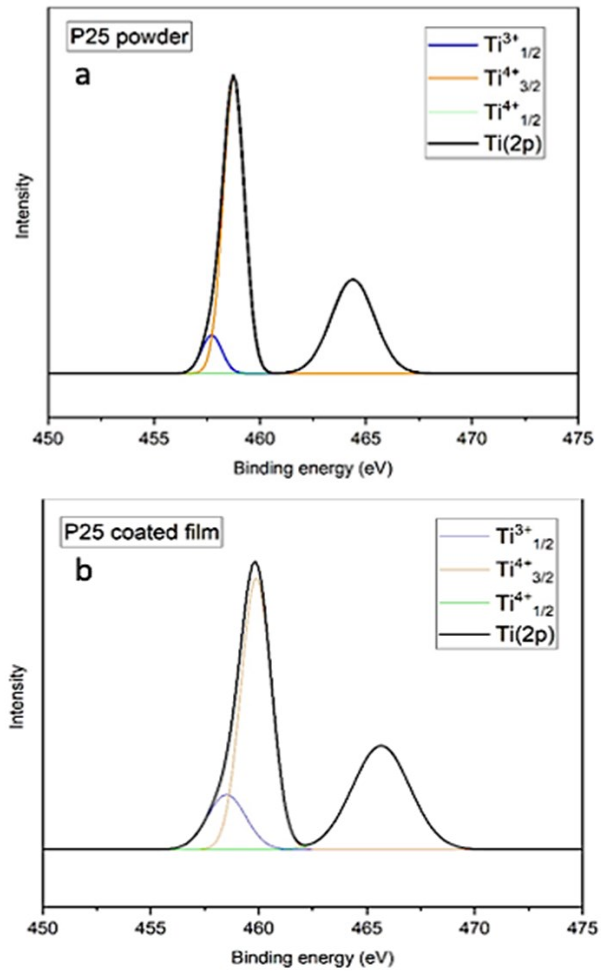

Figure 5. XPS spectra of (a) P25 powder and (b) P25 coated PET film.

The XPS binding energy of element composite in the catalyst was characterized for determining Ti^{3+}/Ti^{4+} ratio of P25 powder and coated P25 film (Figure 5). The binding energy of Titanium (Ti2p), Ti (2p2) at 458.6 eV is Ti^{4+} and Ti (2p1) at 456.8 eV is Ti^{3+} in TiO_2. The result shows that Ti^{3+}/Ti^{4+} ratio is 0.07 and 0.15 for P25 powder and coated P25 film, respectively. Therefore, P25 coated PET film can reduce energy band gap due to it can change oxidation state of Ti^{4+} to Ti^{3+} from bonding P25 with PET surface.

The photoluminescence (PL) measures the efficiency and electrical properties of semiconductors such as charge carrier trapping, carrier lifetime and recombination. The PL spectrum of PET–1.0Si–P25 is provided in Figure 6. The intensity indicates the emission energy of e^-/h^+ recombination rate. Although the main signal occurs at 425 nm, signals of higher wavelengths are also detected, which may be attributed to different traps, including those of the silicate binder and oxygen vacancies (Vo) at 560 nm. The signals have high enough intensities to provide good catalyst light harvesting.

3.2 Methylene Blue Oxidation Test

The methylene blue (MB) absorbance versus plots of TiO_2 (P25) for 1 g without TEOS as a binder and for different volumes of TEOS with 1 g P25 are presented in Figure 7(a). It is clear that for the 1 g P25 sample, faster degradation of MB occurs when using 1 mL TEOS (PET–1.0Si–P25). Since this is an exponential degradation, the pseudo-first-order degradation can

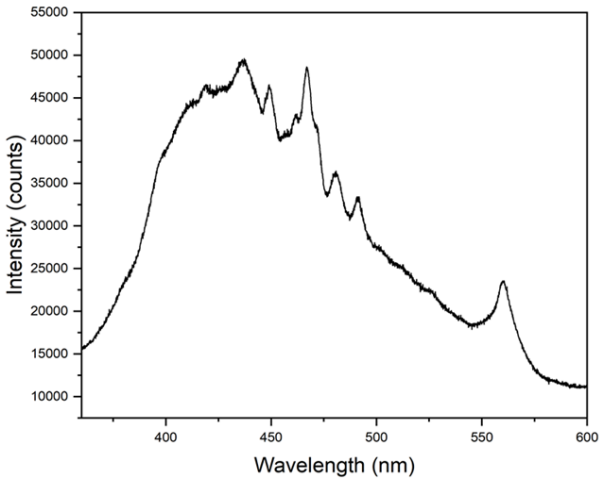

Figure 6. 320 nm excitation photoluminescence spectrum of P25-SiO_2 powder.

be adjusted to the experimental points. Figure 7(b) reveals a plot of $\ln(-(Abs_{inf}-Abs_t))$ versus t, where Abs_{inf} and Abs_t are the corresponding absorbances at an infinite time (when leveling is observed at 120 min) and at time t, respectively. Accordingly, the pseudo-first-order rate constants for the degradation of MB were obtained from the slope of the plot. Besides, both of SEM/EDX characterization and methylene blue degradation show the conformed results explaining Ti active site quantity on film effects to methylene blue degradation efficiency.

Figure 8(a) shows a calibration curve for MB absorbance at 668 nm versus concentration. Using this curve, the concentrations of MB at each time were obtained. Additionally, a plot of $\ln([MB]_t/[MB]_0)$ versus time is presented. From the slope, a value of k_{obs} = 0.023 min^{-1} was obtained, which is similar to that in Figure 8(b). In Table 1, the pseudo-first-order rate constants, the percentage of conversions for the three methods of preparation of the modified film are shown. This table also shows the rate obtained (in $\mu g.mL^{-1}.g_{cat}^{-1}.h^{-1}$) for the fastest MB degradation. The T4 bacteriophage has been used previously to test the activity of glass coated with thin films of TiO, CuO, and CuO/TiO_2, and a direct correlation was identified between the oxidation capacities of these films and the inactivation rate of the virus, as it was pointed out by Ditta *et al.* [7]. Thus, the present study selected the PET–1.0Si–P25–SiO_2 that provides the optimal MB oxidation degradation to test the inactivation of ***Phi–X 174*** using fluorescent and UV lights.

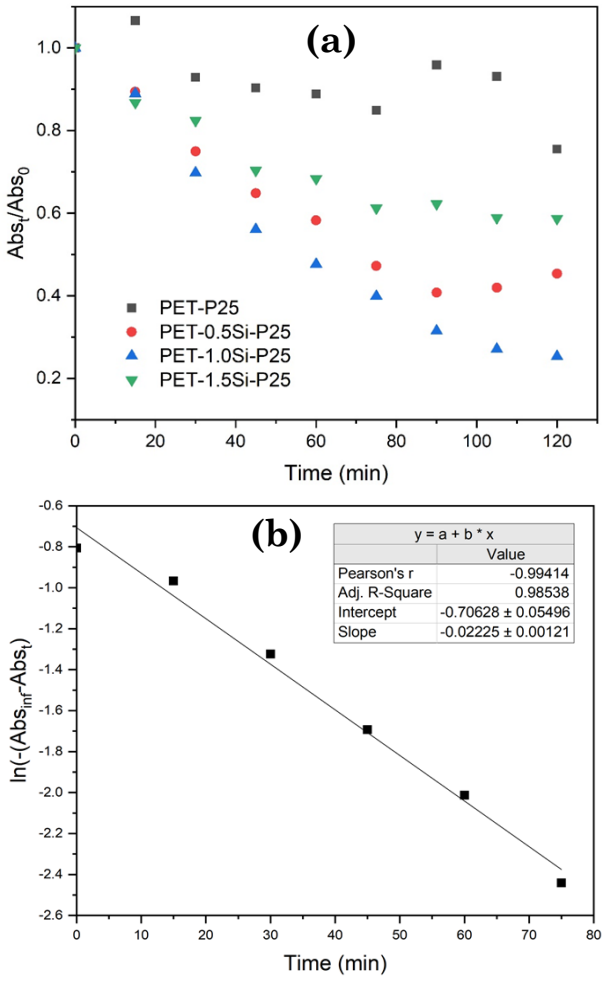

Figure 7. (a) Absorbance vs. t plots of MB degradation using different coated PET films preparation proportions of the P25 (TiO_2) and Tetraethyl ortho silicate (TEOS). $[MB]_0$ = 4 ppm, neutral pH. (b) Plot of ln $(-(Abs_{inf}-Abs_t))$ vs. t for MB degradation using PET-1.0Si-P25. $[MB]_0$ = 4 ppm, neutral pH, k_{obs} = −slope = 0.02 min^{-1}.

3.3 Adsorption Experiments

This study tested the adsorption of MB on PET, PET–0.5Si–P25, PET–1.0Si–P25, and

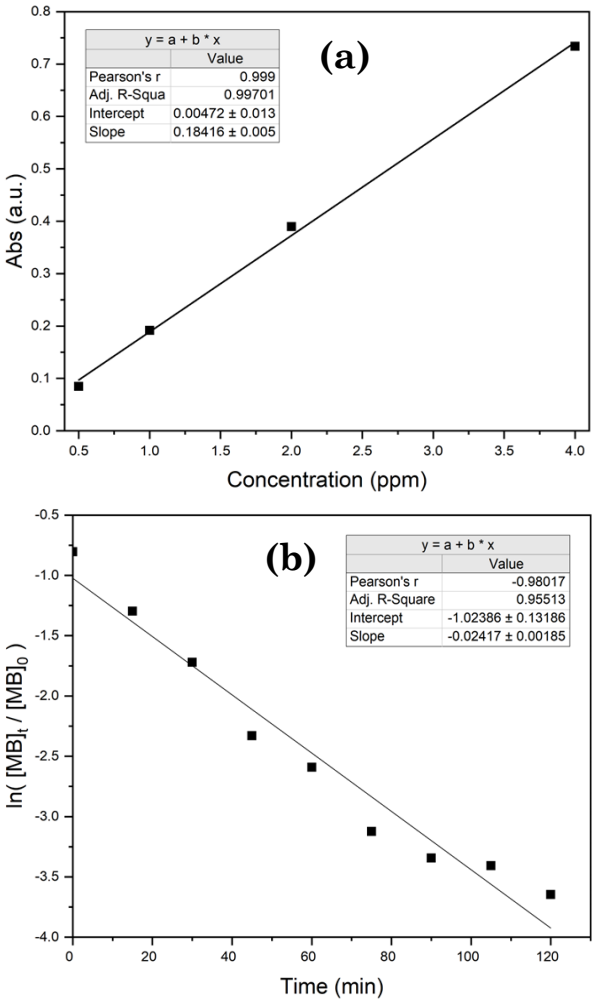

Figure 8. (a) Absorbance vs. [MB] calibration curve. (b) $\ln([MB]_t/[MB]_0)$ vs. t plot. From the slope pseudo-first order rate constant (k_{obs}: min^{-1}) is obtained.

PET–1.5Si–P25 films without light and collected the samples after 10, 30, and 60 min to measure the optimal adsorption time for MB degradation. The results revealed the optimal adsorption time to be 10 min. As shown in Figure 9(a), the PET–1.0Si–P25–SiO_2 film exhibited the highest adsorption ability.

To test the adsorption of ***Phi–X 174*** on film, PET–1.0Si–P25 and PET–1.0Si–P25–SiO_2 were tested without light. Samples were obtained after 10, 30, and 60 min to obtain the optimal adsorption time for the virus. The results revealed this to be 10 min, and the best absorption ability was exhibited using the PET–1.0Si–P25–SiO_2 sample (Figure 9(b)). The highest adsorption of both MB and ***Phi–X 174*** was obtained in the presence of nanosilica.

The reasonable MB and ***Phi–X 174*** adsorption mechanism can result from hydrogen bonding and electrostatic interactions between negatively charged groups on the catalyst in the presence of nanosilica (PET–1.0Si–P25–SiO_2) and cationic MB as well as ***Phi–X 174***.

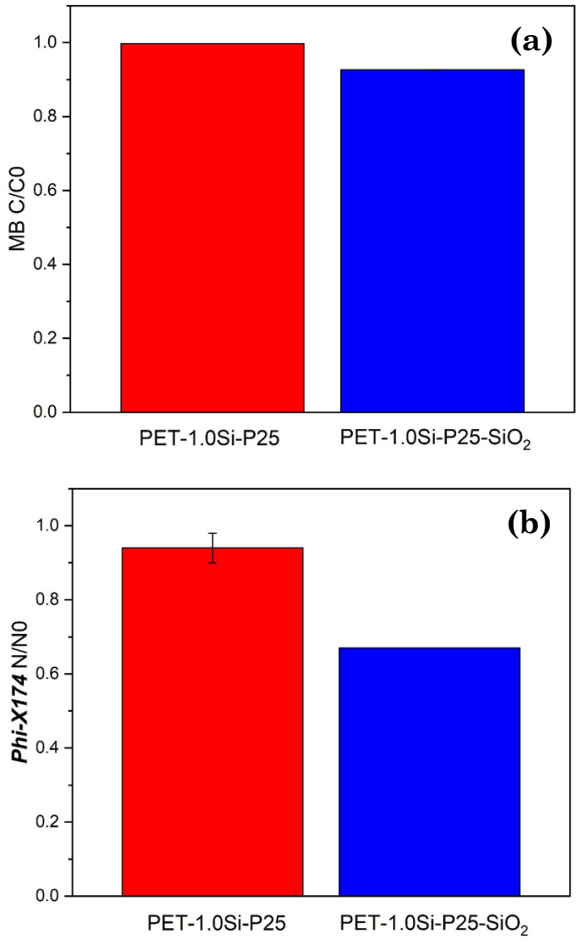

Figure 9. (a) PET-1.0Si-P25 adsorption (no light) of methylene blue. (b) PET-1.0Si-P25-SiO_2 adsorption (no light) of virus ***Phi-X174***.

The proposed adsorbent, PET–1.0Si–P25–SiO_2, includes hydroxyl groups. As it is known, hydroxyl groups can be generally observed non-ionized form at lower pHs, so lower interactions between non-ionized hydroxyl and positively charged are observed which is known as hydrogen bonding interactions. Hence, the adsorption of cationic MB and ***Phi–X 174*** on PET–1.0Si–P25–SiO_2 having negatively charged groups could be more efficient through electrostatic interactions.

3.4 Virus Inactivation Experiments

Since the oxidation of MB increased when the PET–1.0Si–P25 modified film sample was used, this film was also selected for use in the

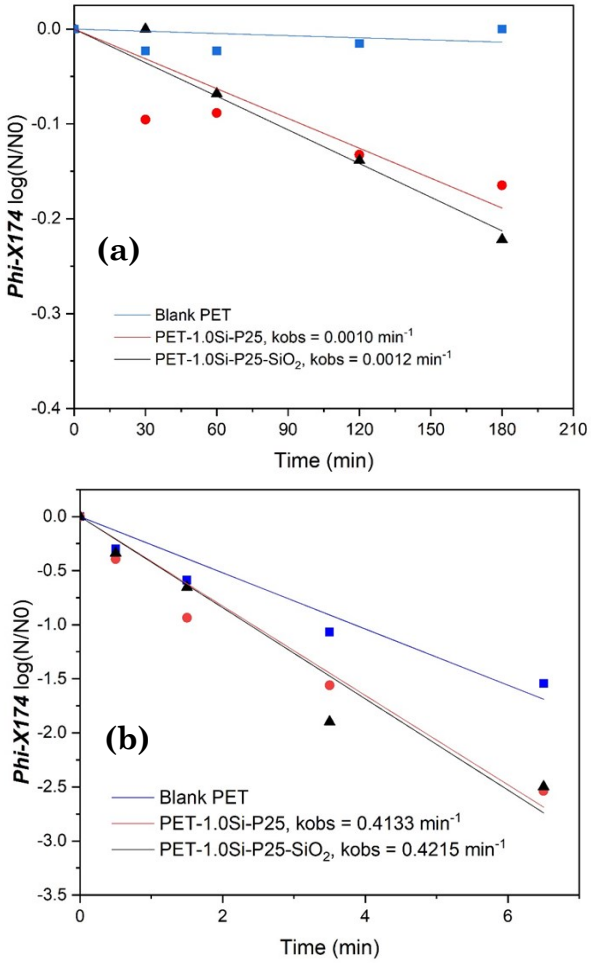

Figure 10. (a) Fluorescence 2000 lux lamp for Virus ***Phi-X 174*** Bacteriophage inactivation using PET (blank), PET-1.0Si-P25, and PET-1.0Si-P25-SiO_2. k_{obs} are obtained from the slopes of log (N/N_0) vs. time plots. N and N_0 are the concentration of virus at time t and the concentration of virus after adsorption but before irradiation, respectively. (b) Same conditions using UV-C 18 W lamp.

Table 2. Fluorescence and UV-C lamps inactivation pseudo-first order rate constants (k_{obs}), % of Virus ***Phi-X 174*** Bacteriophage inactivation, Log reduction and PFU $mL^{-1}.g_{cat}^{-1}.t^{-1}$ using PET, P25 on PET and 5 % added nano SiO_2 with P25 on PET.

Catalyst films total catalyst weight of 103.2 cm^2 of film: 0.005 g	Fluorescence lamp 2000 Lux				UV-C lamp 18 W			
	k_{obs} (min^{-1}) parenthesis: half-time (min)	%Inactivation (1 h)	Log reduction after 3 h	Rate (PFU.$mL^{-1}.g_{cat}^{-1}.min^{-1}$) $\times 10^{-6}$	k_{obs} (min^{-1}) parenthesis: half-time (min)	%Inactivation (0.5 min)	Log reduction after 6.5 min	Rate (PFU $mL^{-1}.g_{cat}^{-1}.min^{-1}$) $\times 10^{-6}$
Blank PET	[a]	[a]	[a]	[b]	0.2598 (1.2)	50	1.5log	[b]
PET-1.0Si-P25	0.0010 (301)	19	0.2 log	4.0	0.4133 (0.7)	59	2.5log	9.6
PET-1.0Si-P25-SiO_2	0.0012 (250)	15	0.2 log	3.7	0.4215 (0.7)	54	2.5log	8.9

[a] Not detectable.
[b] Not catalyst added.

virus inactivation tests. As the addition of SiO_2 has been reported to improve the deactivation of microorganisms [5], the present study included an additional film prepared by adding 5% of nano SiO_2 (PET–1.0Si–P25–SiO_2) to the last preparation method of film preparation. Figure 10(a) shows a plot of the log of N/N_0 versus time, in which N and N_0 are the viral concentrations in PFU.mL^{-1} at time t and concentration after adsorption, respectively. Thus, the values obtained at each time interval indicate the film's virus removal efficiency. The figure includes a PET control sample for comparison. It can be seen that the P25 and PET–1.0Si–P25–SiO_2 films both provide the best removal with fluorescent light. Table 2 shows the k_{obs} obtained from the slopes of Figure 10(a), the percentage of conversions after 30 and 45 min, the log reduction efficiencies, and the rates of virus inactivation in PFU.$mL^{-1}.g_{cat}^{-1}.h^{-1}$. As can be seen in Figure 10(b), under UV light, the deactivation of the virus is faster. However, activity is also observed with the control PET film, which suggests that UV light alone promotes viral deactivation. The k_{obs}, inactivation percentage after 0.5 min of irradiation, log reduction after 6.5 min, and deactivation rate in PFU.$mL^{-1}.g_{cat}^{-1}.min^{-1}$ are all provided. The addition of 5% nano SiO_2 during the preparation of the film provides a virus inactivation efficiency equal to that of the P25 film.

The linear correlation between the OH. and the deactivation of ***E. Coli*** revealed that [22] hydroxyl radicals are the primary oxidation species in microorganism inactivation with UV light. Glass and steel coated with lanthanide- and neodymium-doped TiO_2 have been reported [23] to successfully destroy the foodborne pathogen, Staphylococcus aureus. However, there are few reports of virus inactivation using visible light photocatalysis, particularly in terms of the coexistence of viruses and their host bacteria. Cu–TiO_2 nanofibers under visible light have been investigated [24] under this condition, and the pH and catalyst dosages were found to affect the inactivation rate. A neutral pH was found to be the most effective with doses of >75 mg/L at 25 °C and an initial virus concentration of 10^5 PFU.mL^{-1}. Additionally, the intensity of light has been confirmed to affect the inactivation rate (optimal performance achieved with 130 mW/cm^2). Generally, $-\log(N/N_0)$ approximately 3–5 values are obtained after an irradiation time of 120 min. The present study's results using the PET–1.0Si–P25–SiO_2 film sample achieved 60% inactivation after 1 h (Table 2). However, the virus deactivation rate per gram of catalyst

(0.005 g/film, Table 2) was 4×10^6 PFU.mL^{-1}.g$_{cat}^{-1}$.min^{-1}. Hence, considering the indoor threshold for airborne microorganisms of 500 PFU.m^{-3} [11], a virus deactivation rate of 6.6×10^5 PFU.mL^{-1}.g$_{cat}^{-1}$.h^{-1} is an important goal. However, achieving this requires approximately 1.4×1.4 m (10^3 cm^2/0.005 g)$^{0.5}$ of the film (see Table 2), although the abovementioned threshold may be reached using a smaller area if the contaminated air is forced to contact the film.

In the present study, the experiments were conducted in batches in which virus–bacteria PFUs were added onto films. The control of direct-contact viral contamination could be achieved quite well using the film, as the preliminary detection tests using the Lumitester A3 (ATP+ADP+AMP) confirmed. Additionally, airborne viruses may be deactivated using the film. Although the conditions of airborne viral flows are different from the experiments performed in this study, good agreement between the laboratory results of catalyst oxidation and those of the prototype test was confirmed [11] for glass and steel coated with TiO_2 and P25 using a simple photoreactor with tangential air tested in a chamber and a prototype air purifier. However, when comparing the results for microorganisms, the efficiency of the prototype is reduced, which is likely to be attributed to the protection of microorganisms by the liquid droplets and particulates in natural aerosols.

In the virus model shown in Figure 1, the product with photocatalytic could produce reactive oxygen species (ROS) and have a high potential to induce oxidation reaction with microorganism. When the oxidation between product and virus occurred, the outer membrane of virus is structured by glycoprotein inserted on phosphatidylethanolamine lipids. The figure shows that ROS (OH.) stimulates membrane oxidation [25], which has been confirmed using TiO_2/UV light. Viruses are the most susceptible pathogens to ROS oxidation when TiO_2 and ZnO are used as photocatalysts [26]. This oxidation promotes pore formation, phase separation, and membrane permeability, leading to the deterioration of viruses [27]. The results obtained in the present study confirm that the developed P25 film can protect against viral [22,28–30] contamination from direct contact on surfaces and via transmission in indoor air. Besides, ROS can cause oxidative stress within virus, and extracellular ROS may enter into the virus and cause dramatically boosted ROS levels intracellularly, which would react with antioxidative enzymes, disrupting the balance of oxidation and antioxidation in virus cells [31].

4. Conclusions

This study prepared and tested P25 films to investigate methylene blue (MB) oxidation using UV light. The film prepared with 1 g P25 and 1 mL TEOS (PET–1.0Si–P25) was found to degrade MB faster than the other P25:TEOS ratios tested. A k_{obs} value of 0.02 min^{-1} (half time = 15 min) and a rate of 85 μg.mL^{-1}.g$_{cat}^{-1}$.h^{-1} were measured. Because of the direct correlation between the rates of oxidation and virus deactivation, this film was used to test the removal efficiency of the ***Phi–X174*** virus. The deactivation mechanism of ***Phi–X174*** and other viral models involves the destruction via ROS (mainly hydroxyl radicals) of the virus' membrane; because of the narrow bandgap (2.8 eV) of the film induced by the silicate binder, ROS can be produced using visible light. The presence of nanosilica indicates significant adsorption capacity for both MB and ***Phi–X174***. Irradiation under a fluorescent lamp for 3 h produced a virus removal rate of 0.2 log at a rate of 4×10^6 PFU.mL^{-1}.g$_{cat}^{-1}$.min^{-1}, which is effective in preventing viral contamination via direct contact with surfaces and transmission in indoor air. UV-C light produced a removal of up to 2.5 log after 6.5 min of irradiation. However, the PET control film produced a removal of just 1.5 log. Thus, UV light is efficient at deactivating not only the virus but also the cells of other living organisms. Accordingly, this represents a drawback for using UV light for such applications.

Acknowledgments

We are grateful for the grant support from the National Research Council of Thailand (NRCT).

References

[1] Linsebigler, A., Lu, G., Yates J. (1995). Photocatalysis on TiO_2 surfaces: principles, mechanisms, and selected results. *Chemical Reviews*, 95(3), 735–758. DOI: 10.1021/cr00035a013

[2] Schneider, J., Matsuoka, M., Takeuchi, M., Zhang, J., Horiuchi, Y., Anpo, M., Bahnemann, D. (2014). Understanding TiO_2 photocatalysis: mechanisms and materials. *Chemical Reviews*, 114(19), 9919–9986. DOI: 10.1021/cr5001892

[3] Ollis, D. (2018). Kinetics of photocatalyzed reactions: Five lessons learned. *Frontiers in Chemistry*, 6, 378. DOI: 10.3389/fchem.2018.00378

[4] Zheng, X., Shen, Z., Cheng, C., Shi, L., Cheng, R., Yuan, D. (2018). Photocatalytic disinfection performance in virus and virus/bacteria system by Cu-TiO_2 nanofibers under visible light. *Environmental Pollution*, 237, 452–459. DOI: 10.1016/j.envpol.2018.02.074

[5] Jafry, H., Liga, M., Li, Q., Barron, A. (2011). Simple route to enhanced photocatalytic activity of P25 titanium dioxide nanoparticles by silica addition. *Environmental Science & Technology*, 45(4), 1563–1568. DOI: 10.1021/es102749e

[6] Habibi, A., Asadzadeh, S., Feizpoor, S., Rouhi, A. (2020). Review on heterogeneous photocatalytic disinfection of waterborne, airborne, and foodborne viruses: Can we win against pathogenic viruses?. *Journal of Colloid and Interface Science*, 580, 503–514. DOI: 10.1016/j.jcis.2020.07.047

[7] Ditta, I.B., Steele, A., Liptrot, C., Tobin, J., Tyler, H., Yates, H., Sheel, D., Foster, H. (2008). Photocatalytic antimicrobial activity of thin surface films of TiO_2, CuO and TiO_2/CuO dual layers on Escherichia coli and bacteriophage T4. *Applied Microbiology and Biotechnology*, 79, 127–133. DOI: 10.1007/s00253-008-1411-8

[8] Akhavan, O., Choobtashani, M., Ghaderi, E. (2012). Protein degradation and RNA efflux of viruses photocatalyzed by graphene–tungsten oxide composite under visible light irradiation. *The Journal of Physical Chemistry C*, 116(17), 9653–9659. DOI: 10.1021/jp301707m

[9] Nasralla, N., Yeganeh, M., Astuti, Y., Piticharoenphun, S., Šiller, L. (2018). Systematic study of electronic properties of Fe-doped TiO_2 nanoparticles by X-ray photoemission spectroscopy. *Journal of Materials Science: Materials in Electronics*, 29, 17956–17966. DOI: 10.1007/s10854-018-9911-5

[10] Nasralla, N., Yeganeh, M., Astuti, Y., Piticharoenphun, S., Shahtahmasebi, N., Kompany, A., Karimipour, M., Mendis, B.G., Poolton, N.R.J., Šiller, L. (2013). Structural and spectroscopic study of Fe-doped TiO_2 nanoparticles prepared by sol–gel method. *Scientia Iranica*, 20, 1018–1022. DOI: 10.1016/j.scient.2013.05.017

[11] Yao, N., Yeung, K. (2011). Investigation of the performance of TiO_2 photocatalytic coatings. *Chemical Engineering Journal*, 167, 13–21. DOI: 10.1016/j.cej.2010.11.061

[12] Dutschke, A., Diegelmann, C., Löbmann, P. (2003). Preparation of TiO_2 thin films on polystyrene by liquid phase deposition. *Journal of Materials Chemistry*, 13, 1058–1063. DOI: 10.1039/B212535H

[13] Essawy, A., Ali, A., Abdel-Mottaleb, M. (2008). Application of novel copolymer-TiO_2 membranes for some textile dyes adsorptive removal from aqueous solution and photocatalytic decolorization. *Journal of Hazardous Materials*, 157(2-3), 547–552. DOI: 10.1016/j.jhazmat.2008.01.072

[14] Lu, S., Sun, S., Niu, J., Zeng, L., Liu, H., Zhao, X. (2012). Poly (thienylene methine) grafted nanocrystalline TiO_2 based hybrid solar cells. *Journal of Materials Science: Materials in Electronics,* 23, 251–256. DOI: 10.1007/s10854-011-0397-7

[15] Mesnage, A., Magied, M., Simon, P., Herlin-Boime, N., Jégou, P., Deniau, G., Palacin, S. (2011). Grafting polymers to titania nanoparticles by radical polymerization initiated by diazonium salt. *Journal of Materials Science*, 46, 6332–6338. DOI: 10.1007/s10853-011-5709-z

[16] Tchoul, M., Fillery, S., Koerner, H., Drummy, L., Oyerokun, F., Mirau, P., Durstock, M., Vaia, R. (2010). Assemblies of titanium dioxide-polystyrene hybrid nanoparticles for dielectric applications. *Chemistry of Materials*, 22(5), 1749–1759. DOI: 10.1021/cm903182n

[17] Ye, C., Li, H., Cai, A., Gao, Q., Zeng, X. (2011). Preparation and characterization of organic nano-titanium dioxide/acrylate composite emulsions by in-situ emulsion polymerization. *Journal of Macromolecular Science, Part A*, 48(4), 309–314. DOI: 10.1080/10601325.2011.552353

[18] Klaysri, R., Wichaidit, S., Piticharoenphun, S., Mekasuwandumrong, O., Praserthdam, P. (2016). Synthesis of TiO_2-grafted onto PMMA film via ATRP: Using monomer as a coupling agent and reusability in photocatalytic application. *Materials Research Bulletin,* 83, 640–648. DOI: 10.1016/j.materresbull.2016.07.019

[19] Marcelino, R., Amorim, C., Ratova, M., Delfour-Peyrethon, B., Kelly, P. (2019). Novel and versatile TiO_2 thin films on PET for photocatalytic removal of contaminants of emerging concern from water. *Chemical Engineering Journal*, 370, 1251–1261. DOI: 10.1016/j.cej.2019.03.284

[20] Izumi, I., Hiroyuki, S., Toyoki, K. (1996). Stepwise adsorption of metal alkoxides on hydrolyzed surfaces: A surface sol-gel process. *Chemistry Letters*, 25, 831–832. DOI: 10.1246/cl.1996.831

[21] Nowacka, M., Ambrożewicz, D., Jesionowski, T. (2013). TiO_2-SiO_2/Ph-POSS functional hybrids: Preparation and characterisation. *Journal of Nanomaterials*, 2013, 680821. DOI: 10.1155/2013/680821

[22] Cho, M., Chung, H., Choi, W., Yoon, J. (2004). Linear correlation between inactivation of E. coli and OH radical concentration in TiO_2 photocatalytic disinfection. *Water Research*, 38(4), 1069–1077. DOI: 10.1016/j.watres.2003.10.029

[23] Cushnie, T., Robertson, P., Officer, S., Pollard, P., Prabhu, R., Mccullagh, C., Robertson, J. (2010). Photobactericidal effects of TiO_2 thin films at low temperatures—A preliminary study. *Journal of Photochemistry and Photobiology A: Chemistry*, 216(2-3), 290-294. DOI: 10.1016/j.jphotochem.2010.06.027

[24] Choi, S., Cho, B. (2018). Extermination of influenza virus H1N1 by a new visible-light-induced photocatalyst under fluorescent light. *Virus Research*, 248, 71–73. DOI: 10.1016/j.virusres.2018.02.011

[25] Kiwi, J., Nadtochenko, V. (2004). New evidence for TiO_2 photocatalysis during bilayer lipid peroxidation. *The Journal of Physical Chemistry B*, 108(45), 17675–17684. DOI: 10.1021/jp048281a

[26] Bogdan, J., Zarzyńska, J., Pławińska-Czarnak, J. (2015). Comparison of infectious agents susceptibility to photocatalytic effects of nanosized titanium and zinc oxides: a practical approach. *Nanoscale Research Letters*, 10, 309. DOI: 10.1186/s11671-015-1023-z

[27] Tsubone, T., Baptista, M., Itri, R. (2019). Understanding membrane remodelling initiated by photosensitized lipid oxidation. *Biophysical Chemistry*, 254, 106263. DOI: 10.1016/j.bpc.2019.106263

[28] Ciceri, F., Beretta, L., Scandroglio, A., Colombo, S., Landoni, G., Ruggeri, A., Peccatori, J., D'Angelo, A., Cobelli, F., Rovere-Querini, P., Tresoldi, M., Dagna, L., Zangrillo, A. (2020). Microvascular COVID-19 lung vessels obstructive thromboinflammatory syndrome (MicroCLOTS): an atypical acute respiratory distress syndrome working hypothesis. *Critical Care and Resuscitation*, 22(2), 95–97.

[29] Cui, J., Li, F., Shi, Z. (2019). Origin and evolution of pathogenic coronaviruses. *Nature Reviews Microbiology*, 17, 181–192. DOI: 10.1038/s41579-018-0118-9

[30] Krammer, F. (2020). SARS-CoV-2 vaccines in development. *Nature*, 586, 516–527. DOI: 10.1038/s41586-020-2798-3

[31] Zhou, Z., Li, B., Liu, X., Li, Z., Zhu, S., Liang, Y., Cui, Z., Wu, S. (2021). Recent progress in photocatalytic antibacterial. *ACS Applied Bio Materials*, 4(5), 3909–3936. DOI: 10.1021/acsabm.0c01335